International Journal of Automotive Technology, Vol. 8, No. 5, pp. 563–573 (2007)

1229-9138/2007/036-04

OPTIMUM DESIGN OF AN AUTOMOTIVE CATALYTIC CONVERTER FOR MINIMIZATION OF COLD-START EMISSIONS USING A MICRO GENETIC ALGORITHM

Y. D. KIM[1)] and W. S. KIM[2)*]

[1)]Department of Mechanical Engineering, Hanyang University, Seoul 133-791, Korea
[2)]Department of Mechanical Engineering, Hanyang University, Gyeonggi 426-791, Korea

(Received 6 July 2007; Revised 2 September 2007)

ABSTRACT–Optimal design of an automotive catalytic converter for minimization of cold-start emissions is numerically performed using a micro genetic algorithm for two optimization problems: optimal geometry design of the monolith for various operating conditions and optimal axial catalyst distribution. The optimal design process considered in this study consists of three modules: analysis, optimization, and control. The analysis module is used to evaluate the objective functions with a one-dimensional single channel model and the Romberg integration method. It obtains new design variables from the control module, produces the CO cumulative emissions and the integral value of a catalyst distribution function over the monolith volume, and provides objective function values to the control module. The optimal design variables for minimizing the objective functions are determined by the optimization module using a micro genetic algorithm. The control module manages the optimal design process that mainly takes place in both the analysis and optimization modules.

KEY WORDS : Catalyst, Cold-start, Light-off, Converter, Micro genetic algorithm, Optimization

NOMENCLATURE

A : open frontal area of the monolith, m^2
$a(x)$: catalyst distribution function, m^2 Pt/m^3 monolith
a_o : catalytic surface area per unit monolith volume, m^2 Pt/m^3 monolith
C_d : cell density, cpsi
c_k : concentration of species k, mole fraction
c_p : specific heat capacity, J/(kg·K)
d_h : hydraulic diameter of a channel of the monolith, m
D_k : binary diffusion coefficient of species k in the mixture, m^2/s
$E_{a,i}$: activation energy of reaction i, J/kmol
$f(\overline{X})$: objective function, dimensionless
G : inhibition factor, dimensionless
GSA : geometrical surface area per unit monolith volume, m^2/m^3
h_t : heat transfer coefficient, W/(m^2·K)
$\Delta H_{a,j}$: adsorption heat, J/kmol
ΔH_i : enthalpy of reaction i, J/kmol
k_i : rate constant of reaction i, mol·K/(m^2·s)
$k_{a,j}$: pre-exponential factor of adsorption equilibrium constant, dimensionless
$k_{m,k}$: mass transfer coefficient of species k in the mixture, m/s
$k_{0,i}$: pre-exponential factor of rate constant i, mol·K/(m^2·s)
K_j : adsorption equilibrium constant, dimensionless
L : channel length, m
$\dot{m}$: mass flow rate, kg/s
M_g : molecular weight of exhaust gas, kg/kmol
N_d : number of design variables, dimensionless
N_R : number of reactions, dimensionless
Nu_∞ : limiting Nusselt number, $Nu=h_t \cdot d_h/\lambda_g$
r_i : rate of reaction i, mol/(m^2·s)
R : monolith radius, m
R_g : universal gas constant, J/(mol·K)
Sh_∞ : limiting Sherwood number, $Sh=k_{m,i} \cdot d_h/D_i$
t : time, s
T : temperature, K
ν_{ki} : stoichiometric coefficient of species k in the reaction i, dimensionless
V_m : monolith volume, m^3
w : wall thickness, m
x : axial coordinate, m
$\overline{X}$: vector of the design variables, dimensionless
α : coefficient included in the catalyst distribution

*Corresponding author. e-mail: wskim@hanyang.ac.kr

function a(x), dimensionless
β : coefficient included in the catalyst distribution function a(x), dimensionless
ε : void fraction of the monolith, dimensionless
λ : thermal conductivity, W/(m·K)
ρ : density, kg/m^3

SUBSCRIPTS
0 : initial
g : gas
i : reaction index
in : inlet (superscript)
k : gas species or objective function index
L : lower (superscript)
s : solid
U : upper (superscript)

1. INTRODUCTION

Controlling emissions is not simply a case of engine design and engine management. Exhaust after-treatment is also important, especially for meeting more stringent emission regulations. The achievement of tighter emission standards for gasoline vehicles is based on reduction of cold-start emissions by attaining faster light-off of the catalytic converter. Because automotive catalysts operate inefficiently until they reach their "light-off" temperature (50% conversion) at typically 600 K or higher, roughly 60~80% of the engine-out emissions for a typical vehicle over NEDC and FTP-75 test cycles occurs during the initial cold start phase (Koltsakis and Stamatelos, 1997). Therefore, many attempts have been made to reduce the time needed for catalysts to reach their light-off temperature.

In order to minimize cold start emissions, most studies have invested considerable effort into the development of faster light-off for the catalytic converter. Therefore, various strategies have been considered: a dual catalyst system (Summers *et al.*, 1993), close coupled catalyst system (CCC, Church *et al.*, 1991; Jeong and Kim, 2000), air assist injection system (AAI, Harada *et al.*, 1992), electrical heated catalyst (EHC, Whittenberger and Kubsh, 1990), HC adsorption system (Heimrich *et al.*, 1992), and exhaust gas ignition (EGI, Ma *et al.*, 1992). The aforementioned approaches for accelerating catalyst light-off require the use of supplemental devices, which increase the cost of implementing these strategies. Many numerical and experimental studies have been performed in order to improve the flow distribution of exhaust gas velocity within a monolith, and it has been reported that non-uniform distribution can substantially degrade catalyst light-off performance and can also have a negative influence on the lifetime of the converter (Bella *et al.*, 1991; Kim and Son, 1999). However, the approach mentioned in references (Hauber *et al.*, 1998; Martin *et al.*, 1998; Heibel and Spaid, 1999) has a limited applicability in improving catalyst light-off performance due to the space limitation and the difference of the cross-sectional area between the inlet pipe and the monolith face.

To improve light-off performance and conversion efficiency of catalytic converters, parametric investigations on the effect of various design factors (cell density, wall thickness, length and diameter of the monolith, channel geometry, composition of catalyst and washcoat, axial catalyst distribution etc.) of the monolith have been investigated in a number of numerical and experimental studies (Oh and Cavendish, 1982; Summers *et al.*, 1991; Brisley *et al.*, 1995; Jeong and Kim, 2000, 2001, 2002, 2003). In particular, the effect of non-uniform axial distribution of a fixed amount of catalyst on the performance of the catalytic converter has been examined (Psyllos and Philippopoulos, 1993; Baratti *et al.*, 1997; Melis *et al.*, 1997; Tronci *et al.*, 1999). Psyllos and Philippopoulos (1993) showed that the performance of catalysts with a parabolic axial catalyst distribution is better than monoliths with uniform axial catalyst distribution. The optimal non-uniform distribution of catalyst in a pellet has been investigated by Baratti *et al.* (1997); they reported that the optimal catalyst activity distribution is a Dirac delta function, i.e., for optimum performance, all the active catalyst should be deposited at a specific position within the pellet when the reaction rate depends linearly on the catalyst surface area. Melis *et al.* (1997) examined the effect of an axial distribution of a fixed amount of catalyst on the performance of an isothermal reactor, in which both heterogeneous and homogeneous reactions occur. Finally, optimization of the loading pattern for improving warm-up catalyst performance has been performed by Tronci *et al.* (1999). They showed that a high noble metal surface area in the upstream section of the monolith significantly minimizes the cold start pollutant emissions.

In this paper, optimum design of an automotive catalytic converter for minimization of cold-start emissions using a micro genetic algorithm is performed for two optimization problems, the optimal geometry design of the monolith and the optimal axial catalyst distribution of the catalyst. Here, the optimal geometry design of the catalytic converter is carried out for three optimization problems: a baseline catalyst model (Oh and Cavendish, 1982), a catalyst model with higher inlet gas temperature, and a model with a higher inlet gas flow rate. The optimal design of the monolith geometry has been conducted with consideration of a single objective function, and multi-objective functions are used to determine the optimal axial distribution of the catalyst while keeping the catalytic surface area per unit monolith volume constant.

2. MODEL DESCRIPTION

2.1. Catalyst Model

The monolithic catalytic converters used in automotive exhaust after-treatment systems are comprised of numerous small channels which induce a laminar flow field inside. The catalytic material is impregnated on a washcoat, a porous high surface area material, which covers the channels of the substrate along the wetted perimeter. The physical and chemical processes in a monolithic reactor are depicted in Figure 1.

The diffusion of reactants through the gas phase and the porous washcoat is followed by catalytic reactions, which occur on precious metal surface sites at the gas-solid interface inside the porous washcoat. The energy balance of the solid is affected by diffusive transport (conduction) as well as chemical reactions (reaction enthalpy). To solve the energy conservation equations for the solid phase, transient one-dimensional heat conduction is considered in this study. The heat losses to the environment via convection and radiation are negligible, and the heat losses from the front and the rear face of the monolith are neglected. The velocity distribution and temperature profiles of the exhaust gas at the inlet of the monolith are considered to be uniform. The energy (T_s) and mass (c_s) balances for the solid phase are described as

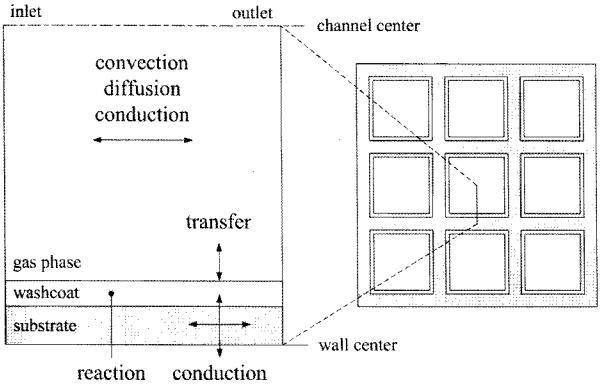

Figure 1. Relevant physical and chemical phenomena in the gas phase, washcoat, and substrate.

$$(1-\varepsilon)\cdot\rho_s\cdot\frac{\partial(c_{p,s}\cdot T_s)}{\partial t}=(1-\varepsilon)\cdot\lambda_s\cdot\frac{\partial^2 T_s}{\partial x^2}- h_t\cdot GSA\cdot(T_s-T_g)+a(x)\cdot\sum_{i=1}^{N_R}(-\Delta H_i)\cdot r_i \quad (1)$$

$$\frac{\rho_g}{M_g}\cdot k_{m,k}\cdot GSA\cdot(c_{k,g}-c_{k,s})=a(x)\cdot\sum_{i=1}^{N_R}\nu_{ki}\cdot r_i \quad (2)$$

where ε, h_t, GSA, a(x), N_R, k_m, and ν_{ki} represent the void fraction of the monolith, the heat transfer coefficient, the geometrical surface area per unit monolith volume, the catalytic surface area per unit monolith volume, the number of reactions, the mass transfer coefficient, and the stoichiometric coefficient of species k in reaction i, respectively.

Using the quasi-steady-state approximation and neglecting diffusion and accumulation terms, the energy (T_g) and mass (c_g) balances for the gas phase become

$$\frac{\dot m}{A}\cdot c_{p,g}\cdot\frac{\partial T_g}{\partial x}=h_t\cdot GSA\cdot(T_s-T_g) \quad (3)$$

$$\frac{\dot m}{A}\cdot\frac{\partial c_{k,g}}{\partial x}=\rho_g\cdot k_{m,k}\cdot GSA\cdot(c_{k,s}-c_{k,g}) \quad (4)$$

To estimate the heat and mass transfer coefficient at constant wall flux, the asymptotic values of the Nusselt and Sherwood numbers of the same magnitude are used (Oh and Cavendish, 1982):

$$h_t=\frac{Nu_\infty\cdot\lambda_g}{d_h} \quad (5)$$

$$k_{m,k}=\frac{Sh_\infty\cdot D_k}{d_h} \quad (6)$$

where $Nu_\infty=Sh_\infty=3.608$ and the diffusivity of species, D_k is estimated using the Slattery-Bird formula (Bird *et al.*, 1960). The inlet and boundary conditions for solving the aforementioned governing equations are:

$$T_s(x,t=0)=T_s^0 \quad (7)$$

$$c_{k,g}(x=0,t)=c_{k,g}^{in} \quad (8)$$

$$T_g(x=0,t)=T_g^{in} \quad (9)$$

Table 1. Rate and adsorption constants adopted in the chemical model.

i, j	Rate constants k_i		Adsorption constants K_j	
	Rate factor $k_{0,i}$ [mol·K·s^{-1}·m^{-2}Pt]	Activation energy $E_{a,i}$ [J/mol]	Adsorption factor $k_{a,j}$ [dimensionless]	Adsorption heat $\Delta H_{a,j}$ [J/mol]
1	6.699×10^{13}	1.040×10^{5}	65.5	−7990
2	1.392×10^{15}	1.210×10^{5}	2.08×10^{3}	-3×10^{3}
3	4.375×10^{13}	1.376×10^{5}	3.98	-9.65×10^{4}
4	6.699×10^{13}	1.040×10^{5}	4.79×10^{5}	3.1×10^{4}

$$\frac{\partial T_s(x=0,t)}{\partial x}=\frac{\partial T_s(x=L,t)}{\partial x}=0 \quad (10)$$

2.2. Chemical Reaction Kinetics Model

The main oxidation reactions, which occur in three-way catalysts, involve carbon monoxide (CO) and unburned hydrocarbons (HC) that are represented by two different species. Propylene (90%) and methane (10%) are used to model "fast" and "slow" oxidizing hydrocarbons, respectively. Due to the substantial heat production associated with hydrogen (H_2) oxidation, this reaction is considered as well (Oh and Cavendish, 1982). In the present model, the oxidation reaction rates of CO, H_2, and HC are based on the expressions developed by Voltz *et al.* (1973). The oxidation reaction scheme over Pt considered in this study is the following:

$$CO+1/2O_2 \rightarrow CO_2,\ \Delta H=-2.832\times10^5 \quad (11)$$

$$C_3H_6+9/2O_2 \rightarrow 3CO_2+3H_2O,\ \Delta H=-1.928\times10^6 \quad (12)$$

$$CH_4+2O_2 \rightarrow CO_2+2H_2O,\ \Delta H=-6.420\times10^5 \quad (13)$$

$$H_2+1/2O_2 \rightarrow H_2O,\ \Delta H=-2.420\times10^5 \quad (14)$$

The expressions of the reaction rates adopted in the chemical model described above are as follows:

$$r_i=\frac{k_i \cdot c_{i,s} \cdot c_{5,s}}{G};\ i=1 \text{ to } 4 \quad (15)$$

$$r_5=0.5 \cdot r_1+4.5 \cdot r_2+2 \cdot r_3+0.5 \cdot r_4 \quad (16)$$

where i=1 (CO), 2 (C_3H_6), 3 (CH_4), 4 (H_2), 5 (O_2), and

$$G=T_s \cdot (1+K_1 \cdot c_{CO,s}+K_2 \cdot c_{HC,s})^2 \cdot (1+K_3 \cdot c_{CO,s}^2 \cdot c_{HC,s}^2) \cdot (1+K_4 \cdot c_{NO,s}^{0.7}) \quad (17)$$

where $k_i=k_{0,i} \cdot \exp(-E_{a,i}/R_gT_s)$ is the rate constant, G is the inhibition factor introduced to consider adsorption and desorption phenomena on the catalytic surface at temperature T_s, and $K_j=k_{a,j} \cdot \exp(-\Delta H_{a,j}/R_gT_s)$ is the adsorption constant. The rate constants k_i and adsorption constants K_j used in this study are given in Table 1 (Oh and Cavendish, 1982).

2.3. Numerical Solution

The governing Equations (1), (3), and (4) are discretized with the finite volume method and solved in conjunction with the initial and boundary conditions given by Equations (7)~(10). The first-order forward difference scheme is used for the first-order spatial derivatives in the gas phase energy and mass Equations (3) and (4) with a midpoint rule applied. A second-order Newton-Raphson method is used for each grid point along the monolith to solve the nonlinear systems of Equations (2), (3), and (4) for $c_{k,s}$, T_g, and $c_{k,g}$. The nonlinear partial differential

Table 2. Input data for catalyst simulation.

Substrate		
Frontal area, A	: 6.0×10^{-3}	m^2
Length, L	: 0.1	m
Cell density, n_c	: 300	cpsi
Wall thickness, w	: 2.54×10^{-4}	m
Hydraulic diameter, d_h	: 1.2×10^{-3}	m
Void fraction, ε	: 0.6836	–
Catalytic surface area per unit monolith volume, a_o	: 26,895	m^2/m^3
Initial temperature, T_s^o	: 300	K
Thermal conductivity, λ_s	: 1.675	W/(m·K)
Density, ρ_s	: 2,500	kg/m^3
Heat capacity, $c_{p,s}$	: $1{,}071+0.156 \cdot T_s-3.435\times10^7/T_s^2$	J/(kg·K)
Exhaust gas		
Mass flow rate,	: 0.04, 0.06	kg/s
Heat capacity, $c_{p,g}$	: 1,089	J/(kg·K)
Thermal conductivity, λ_g	: $2.269\times10^{-4} \cdot T_g^{0.832}$	W/(m·K)
Inlet temperature, T_g^{in}	: 600, 700	K
Inlet concentration of species, $c_{i,g}^{in}$	CO : 2% C_3H_6 : 450 ppm CH_4 : 50 ppm H_2 : 0.667% O_2 : 5% NO : 500 ppm	

Equation (1) is discretized by using a dense uniform grid and employing the control volume approach, the backward difference scheme in time, and the central implicit difference scheme in the spatial direction. The equations are solved by using a standard tri-diagonal matrix algorithm (TDMA) with a successive line under-relaxation scheme.

The physicochemical properties and input data used for the calculations are summarized in Table 2 (Oh and Cavendish, 1982).

Figure 2 compares the computed wall temperature, conversion efficiency of CO, HC, and H_2, and CO cumulative emissions obtained from the current study with the values obtained by Oh and Cavendish (1982) for an inlet gas temperature of 600 K and an exhaust gas flow rate of 0.04 kg/s. As shown in Figure 2, the present numerical results agree well with those of Oh and Cavendish (1982). Also, it can be shown that the CO cumulative emissions at the outlet of the monolith dramatically increase until catalyst light-off (that is, 50% conversion efficiency), and then the rate of CO cumulative emissions decreases due to the instantaneous exothermic reaction in the Pt catalyst. The figure shows that the CO cumulative emissions are approximately 40 g during the initial cold start phase of 200 sec.

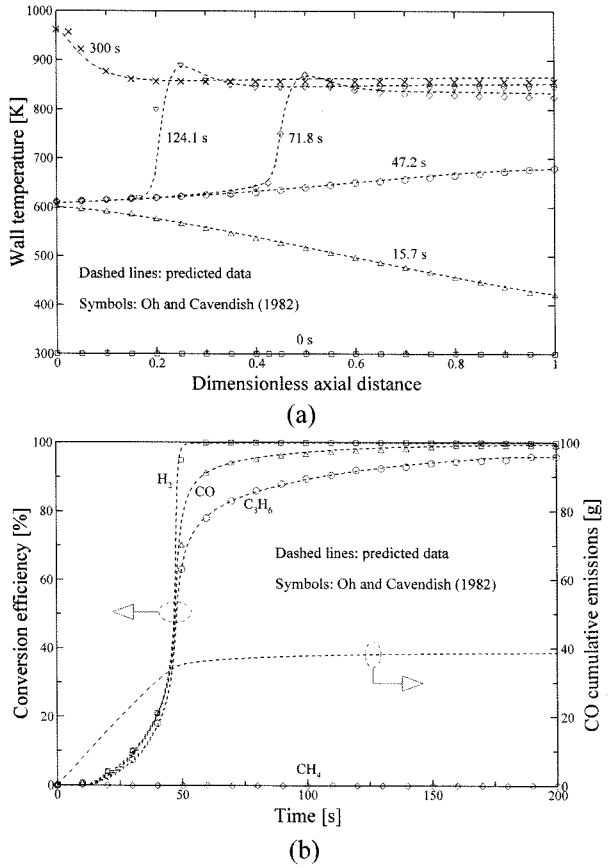

Figure 2. Transient profiles of the wall temperature, conversion efficiencies of the species (CO, C_3H_6, CH_4, and H_2), and CO cumulative emissions for the catalytic converter with T_g^{in}=600 K and $\dot{m}$=0.04 kg/s: (a) wall temperature; (b) conversion efficiency, and CO cumulative emissions.

3. OPTIMIZATION

3.1. Micro Genetic Algorithm

A micro genetic algorithm (μGA) is an optimization technique closely related to GA. μGA works the same way as standard GA (SGA), except that once all the members of a generation have converged within about 5% of each other, the best design is automatically selected for the next generation and the other designs are discarded (Chakravarty *et al.*, 2002). The best design participates in the next generation with new randomly selected designs and the evolutionary process continues. In order to take advantage of μGA's restarting feature, a smaller population size than that for SGA is used. A typical SGA population size is usually about 100 members, where μGA functions best with a population size of about 10 (Chakravarty *et al.*, 2002). Because μGA is repeatedly making random selections, mutation is not used when performing μGA optimization. The flow chart on the right-hand side of Figure 3 depicts the μGA process used in this study. In this study, a population size of 20 with a 50% crossover probability is used. The search process is carried out for 50 generations to see how the objective value varies with the number of evaluations.

3.2. Optimization Procedure and Problem Formulation

The optimum design of an automotive catalytic converter for minimization of cold-start emissions using the micro genetic algorithm is performed for two optimization problems, which are the optimal geometry design of the monolith and the optimal axial catalyst distribution. A flow chart of the optimal design process is depicted on the left-hand side of Figure 3. The optimal design variables of the catalytic converter are obtained through three modules: analysis, optimization, and control. The analysis module is used to calculate the objective functions with a one-dimensional single channel model and the Romberg integration method (Zarowski, 2004). This module obtains new design variables from the control module, produces the CO cumulative emissions and the integral value of a catalyst distribution function a(x) over the monolith volume, and provides objective function values to the control module. The optimal design variables for minimizing the objective functions are determined by the optimization module with μGA. The control module manages the optimal design process that takes place mainly in the analysis and optimization modules. The general mathematical formulation of the nonlinear optimization problem is as follows:

$$\text{find } \bar{X}=\{X_1, X_2, \ldots, X_{N_d}\}^T \tag{18}$$

$$\text{to minimize } \sum_{k=1}^{n} f_k(\bar{X}) \tag{19}$$

$$\text{subject to } \bar{X}^L \le \bar{X} \le \bar{X}^U \tag{20}$$

where $\bar{X}$ is the vector of the design variables containing the cell density (C_d), length (L) and radius (R) of the monolith, and wall thickness (w) that define the optimal geometry of the monolith, α and β are coefficients included in the catalyst distribution function a(x) used to determine the optimal axial distribution of the catalyst, and $f(\bar{X})$ is the objective function.

As mentioned before, two objective functions are considered in this study and described as follows:

$$CCE=\int_0^{t=20 \text{ or } 100 \text{ sec}} CE\ dt \tag{21}$$

$$CSA=\left\{\left[a_o-\frac{1}{V_m}\int^{V_m} a(x)dV_m\right]^2\right\}^{1/2} \tag{22}$$

with

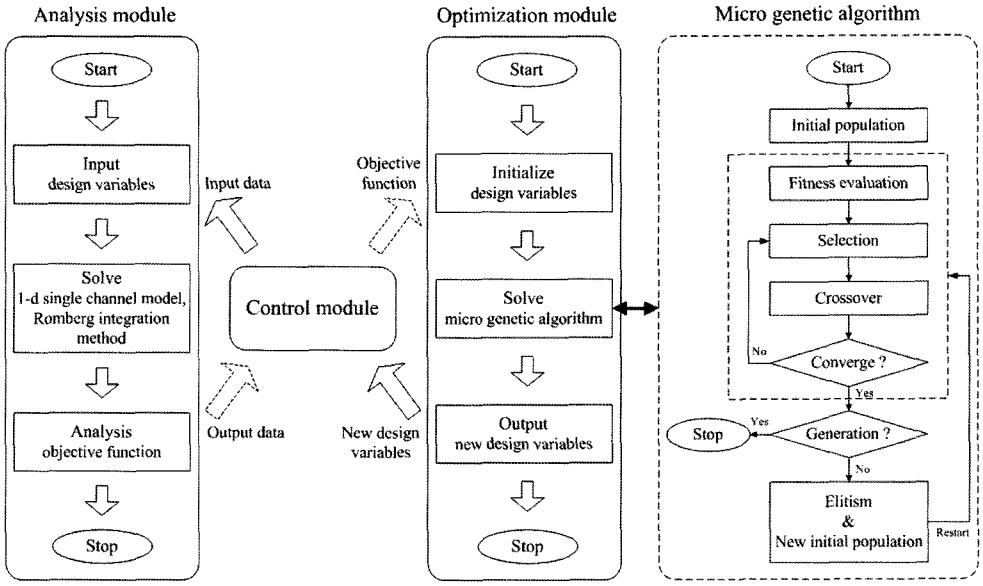

Figure 3. Flow chart of the optimal design process and micro genetic algorithm.

$$a(x)=\exp(\alpha-\beta\cdot x) \tag{23}$$

where CE, V_m, CCE, and CSA are the CO emissions per unit time, monolith volume, along with objective functions $f_1(\bar{X})$ and $f_2(\bar{X})$. $f_1(\bar{X})$ represents the CO cumulative emissions during the initial cold start phase of 20 sec (only for the higher inlet gas temperature, 700 K) or 100 sec. $f_2(\bar{X})$ indicates the difference between the integral value of a catalyst distribution function a(x) over the monolith volume and catalytic surface area per unit monolith volume a_o. α and β are the coefficients included in the catalyst distribution function a(x). These variables are restricted to the lower and upper bounds $\bar{X}^L$ and $\bar{X}^U$ shown in Table 3. The objective functions, design variables, and bounds of the design parameters for two optimization problems and the geometry parameters of the baseline catalyst model (Oh and Cavendish, 1982) are shown in Table 3. The design variables illustrated in Table 3 are determined within a range that can be fabricated with reasonable ease.

Table 3. Objective functions, design variables, and constraints for two optimization problems.

	Geometry optimization of the monolith	Axial distribution optimization of the catalyst
Objective functions, $f(\bar{X})$	CCE	CCE, CSA
Design variables, $\bar{X}$	C_d, L, R, w	α, β
Constraints, $\bar{X}^L \le \bar{X} \le \bar{X}^U$	$0 \le C_d$ [cpsi] ≤ 900 $0 \le$ L [m] ≤ 0.2 $0 \le$ R [m] ≤ 0.05 $10^{-4} \le$ w [m] $\le 5\times10^{-4}$	$-10 \le \alpha \le 10$ $-10 \le \beta \le 10$
Geometry parameters of the baseline catalyst model	C_d=300 cpsi, L=0.1 m, R=0.0437 m, w=2.54×10^{-4} m, α=5.595, β=0	

4. RESULTS AND DISCUSSION

4.1. Optimal Design for the Baseline Catalyst Model

The geometry optimization of the monolith is performed for the baseline monolithic catalyst model listed in Table 3 during the first 100 sec. The temporal evolution of the axial solid temperature profile, conversion efficiency, and CO cumulative emissions of the optimal monolith geometry are illustrated in Figure 4 at an inlet gas temperature of 600 K and exhaust gas flow rate of 0.04 kg/s. Here, the optimal geometry of the monolith consists of C_d=116 cpsi, L=0.2 m, R=0.05 m, and w=10^{-4} m. It can be seen that the optimal design process is carried out by maximizing the catalyst volume, minimizing the wall thickness, and decreasing the cell density compared to the baseline catalyst model. That is, increasing the monolith volume increases the reaction surface area, which leads to an increase in the substrate thermal capacity of the monolith which allows more time to reach the light-off temperature. However, the decreases in the wall thickness and cell density dominate the competitive effect of the increased thermal capacity of the monolith. As shown

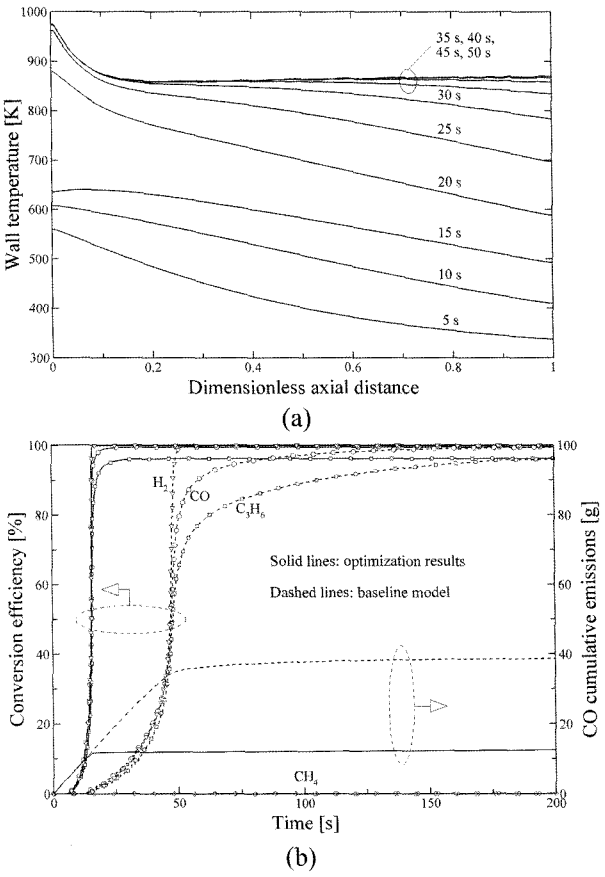

Figure 4. Transient thermal and conversion characteristics of the optimal monolith geometry for the baseline model with T_g^{in}=600 K and $\dot{m}$=0.04 kg/s: (a) wall temperature; (b) conversion efficiency and CO cumulative emissions.

in Figure 4, the solid temperature over the entire monolith region, without the temperature peak in the solid phase during the warm-up, reaches a steady-state in approximately 47 sec; the light-off time and CO cumulative emissions for optimal geometry of the monolith are reduced by approximately 67% and 68%, respectively, compared to the light-off time and CO cumulative emissions obtained from the baseline catalyst model.

To substantiate the validity of the optimization results, the effect of cell density on the CO cumulative emissions and light-off time behavior of a monolith is depicted in Figure 5. Here, the other optimal design variables are kept constant. The behavior depicted in Figure 5 shows that the light-off time gradually decreases as the cell density decreases. However, CO cumulative emissions slightly decrease until the optimal cell density of 116 cpsi is reached and then emissions increase significantly with decreasing cell density due to the degradation of the catalyst's activity after light-off, i.e., the steady-state performance.

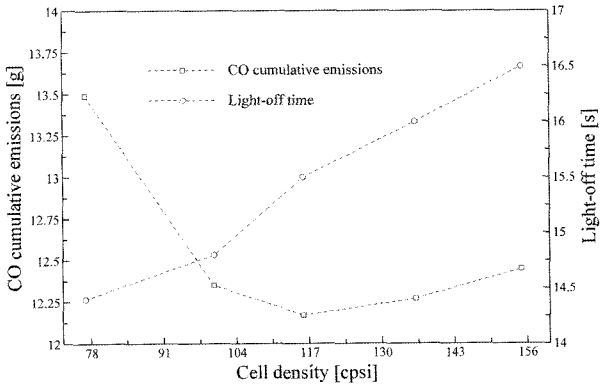

Figure 5. CO cumulative emissions and light-off time with respect to cell densities during the first 100 sec.

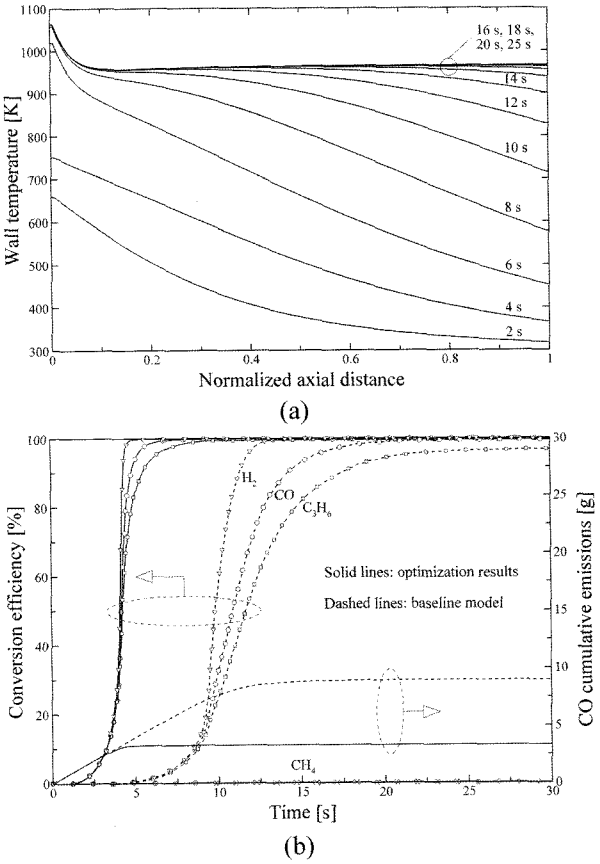

Figure 6. Transient thermal and conversion characteristics of the optimal monolith geometry for the baseline model with T_g^{in}=700 K and $\dot{m}$=0.04 kg/s: (a) wall temperature; (b) conversion efficiency and CO cumulative emissions.

4.2. Optimal Design for the Higher Inlet Gas Temperature

The geometry optimization of the monolith for the baseline catalyst model, with inlet gas temperature of 700 K and flow rate of 0.04 kg/s, is conducted during the first

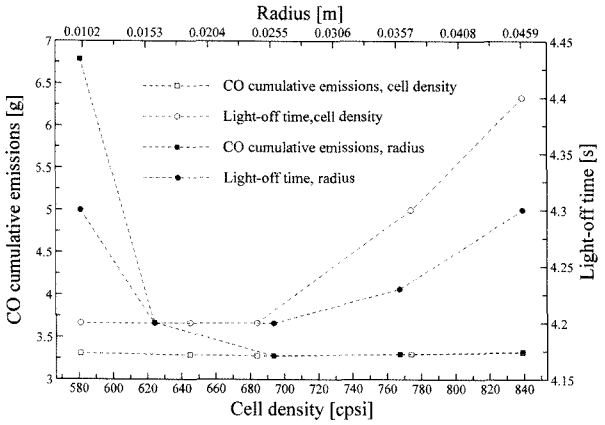

Figure 7. CO cumulative emissions and light-off time with respect to cell density and radius during the first 20 sec.

20 sec. Figure 6 shows the time variation of the wall temperature profile, conversion efficiency, and CO cumulative emissions for the optimal geometry of the catalyst. Here, the optimal design variables of the monolith with C_d=684 cpsi, L=0.1985 m, R=0.0257 m, and w=10^{-4} m are obtained as a result of the optimization investigation.

The optimal design, except for the design variables of cell density and radius, is identically performed with the optimization process mentioned earlier. As the inlet gas temperature is increased from 600 K to 700 K, the light-off performance of the catalyst reverses; that is, faster catalyst light-off occurs with higher cell density and smaller monolith radius. This is because the light-off performance of the catalyst is mainly dominated by the convective heat transfer between gas and solid phases rather than by the heat capacity of the solid phase. In this case, therefore, a fast light-off of the catalyst is favored by the high cell density as a result of the attendant decrease in the hydraulic diameter of the channel. As illustrated in Figure 6, the wall temperature profile over the entire monolith reaches a steady-state at approximately 20 sec and the light-off time and CO cumulative emissions for optimal geometry of the monolith are reduced by approximately 62% and 63%, respectively, compared to those of the baseline catalyst model.

Figure 7 shows how the CO cumulative emissions and light-off time characteristics of a monolithic catalyst are influenced by the cell density and radius of the monolith during the first 20 sec. Here, the other optimal design parameters are kept constant. The CO cumulative emissions have a minimum value at a cell density of 684 cpsi within a small range from 3.28 g to 3.32 g, although the variation of CO cumulative emissions for varying the cell density is negligibly small. The light-off time of the monolith is gradually delayed for cell densities above 684 cpsi because increasing the cell density increases the thermal capacity of the monolith. When the monolith radius is decreased from the optimal value, 0.0257 m, both CO cumulative emissions and light-off time increase due to the attendant decrease in the residence time of gas within the monolith. The CO cumulative emissions and light-off time slightly increase within the range between 3.28 g and 3.33 g and within the range 4.2 sec and 4.3 sec, respectively, when the monolith radius is larger than the optimal value.

4.3. Optimal Design for the Higher Inlet Gas Flow Rate

Here, we examine how the optimal geometry design of the monolith is influenced by a relatively higher mass flow rate (0.06 kg/s) of the exhaust gas at an inlet gas temperature of 600 K during the first 100 sec. Figure 8 shows the transient wall temperature profile, conversion efficiency, and CO cumulative emissions for the optimal catalyst geometry having a cell density of 163 cpsi, length of 0.2 m, radius of 0.05 m, and wall thickness of

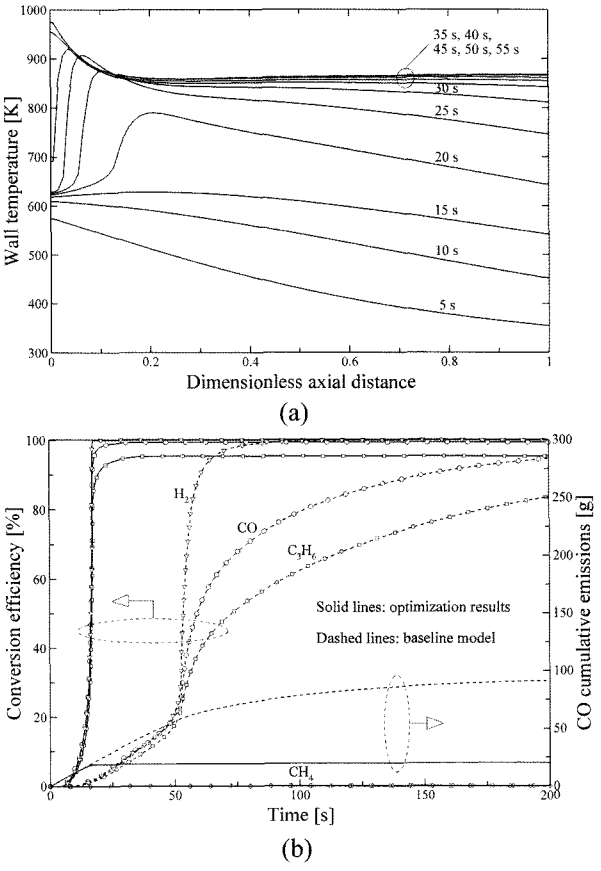

Figure 8. Transient thermal and conversion characteristics of optimal monolith geometry for the baseline model with T_g^{in}=600 K and $\dot{m}$=0.06 kg/s: (a) wall temperature; (b) conversion efficiency and CO cumulative emissions.

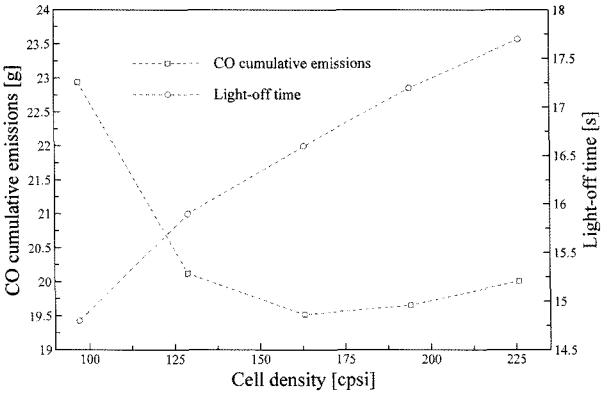

Figure 9. CO cumulative emissions and light-off time with respect to cell densities during the first 100 sec.

10^{-4} m. We can see that the temperature peak develops in the solid phase after catalyst light-off, and then this temperature peak moves rather rapidly toward the inlet of the monolith. The wall temperature over the entire monolith region reaches a steady-state in approximately 50 sec; the light-off time and CO cumulative emissions for optimal monolith geometry are reduced by approximately 72% and 75%, respectively, compared to those of the baseline catalyst model shown in Figure 8. In general, it can be seen that light-off performance of the catalyst deteriorates when it is compared to that observed at a gas flow rate of 0.04 kg/s, primarily due to the attendant decrease in the contact time between the catalyst and exhaust gas.

The effect of exhaust gas flow rate on cumulative CO emissions and light-off time of the monolith is depicted in Figure 9. The light-off time of the catalyst is gradually shortened due to the decreased thermal capacity of the monolith with decreasing the cell density. However, CO cumulative emissions significantly increase after attaining the minimum value of approximately 19.5 g at a cell density of 163 cpsi because catalyst activity deteriorates appreciably after light-off.

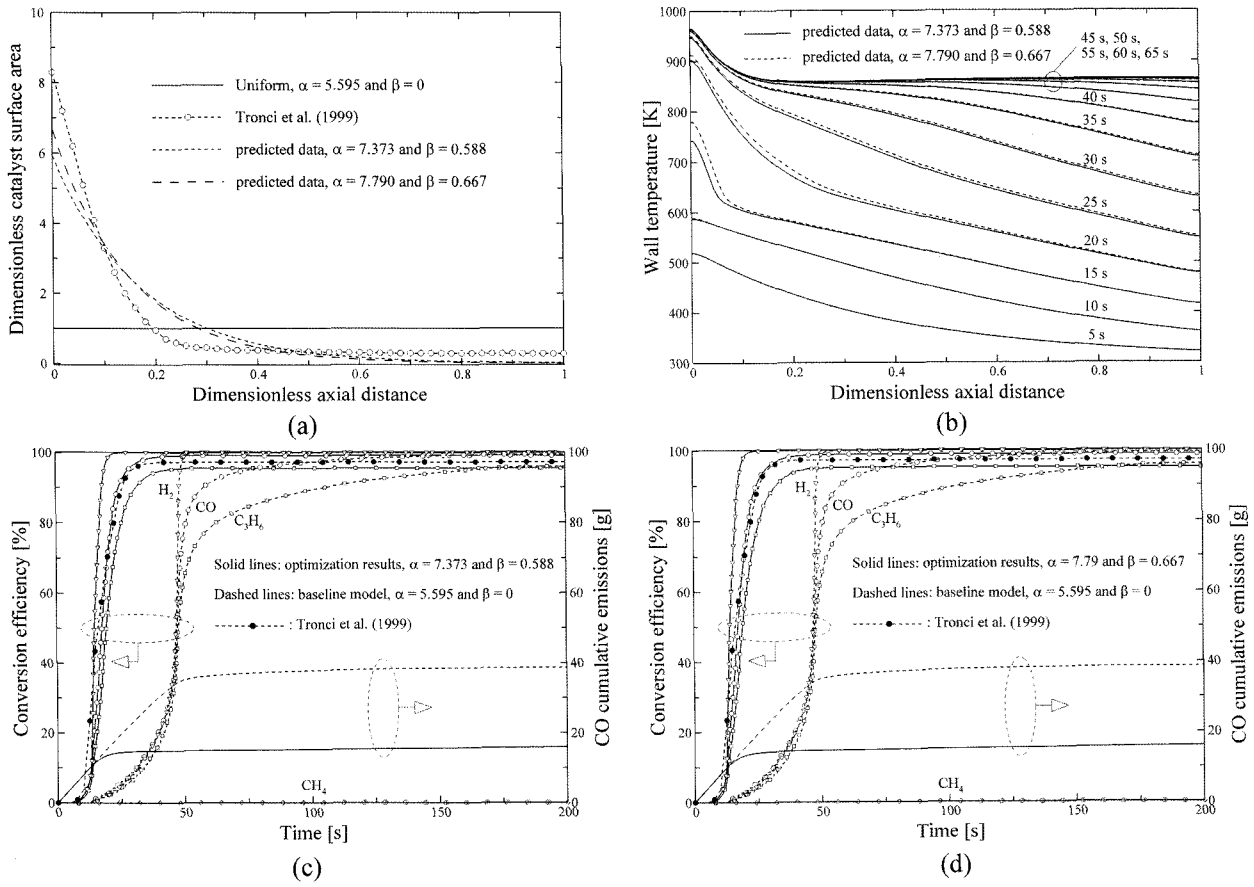

Figure 10. Transient thermal and conversion characteristics of the optimal catalyst distributions for the baseline model with T_g^{in} =600K, $\dot{m}$ =0.04 kg/s, α=5.595, and β=0: (a) optimal catalyst distributions; (b) wall temperature; (c) conversion efficiency and CO cumulative emissions (α=7.373, and β=0.588); (d) conversion efficiency and CO cumulative emissions (α=7.79, and β=0.667).

4.4. Optimal Design for the Axial Catalyst Distribution
The optimal design for the optimal axial distribution of the catalyst is determined by solving the multi-objective optimization problems which are aimed at minimizing the CCE and CSA. Here, the optimization parameters are the coefficients (α, β) included in the catalyst distribution function a(x), as can be seen from Equation (23).

Figure 10 depicts the optimal catalyst distributions, the temporal evolution of axial solid temperature profile, conversion efficiency, and cumulative CO emissions for the optimal axial catalyst distributions along the monolith at an inlet gas temperature of 600 K and exhaust gas flow rate of 0.04 kg/s. Here, the optimal coefficients α and β are 7.373 and 0.588 for case I, and 7.79 and 0.667 for case II, respectively, and the integral value of the catalyst distribution function a(x) over the monolith volume is 26,983 m^2/m^3 for case I and 26,822 m^2/m^3 for case II. As shown in Figure 10(a), the catalyst surface area of the optimal distributions is higher in the upstream section. The catalyst surface area in the downstream section is lower than that of the uniform distribution and that determined by Tronci *et al.* (1999). Also, it can be seen that the concentration degree of the catalyst surface area in the upstream section for both optimal catalyst distributions is lower than that obtained by Tronci *et al.* (1999).

As illustrated in Figure 10(b), the light-off performance of the monolith for case II is slightly better than that of case I, but in both, a steady-state is reached at approximately 60 sec. Although the light-off times of the monolith having optimal catalyst distribution are delayed by approximately 1 sec compared to the light-off time of 16 sec from Tronci *et al.* (1999), the steady-state performances of the catalyst are better compared to that of Tronci *et al.* (1999). Therefore, the light-off time and cumulative CO emissions for both optimal catalyst distributions are approximately 63% and 60% lower compared to light-off times and cumulative CO emissions obtained with the uniform catalyst distribution, respectively.

5. CONCLUSIONS

In this study, the optimal design of the automotive catalytic converter for minimization of cold-start emissions using a micro genetic algorithm is numerically performed to obtain the optimal geometry design of a monolith under various operating conditions and optimal axial catalyst distribution of the catalyst. The following conclusions can be drawn from the optimization of the catalytic converters.

(1) In the optimal design for the baseline catalyst model, it can be seen that the decreases in the wall thickness and cell density are the major factors for the increased thermal capacity of the monolith. The increased thermal capacity is due to the increase of the monolith volume which increases the reaction surface area. Here, the light-off time and cumulative CO emissions are reduced by approximately 67% and 68%, respectively, as compared to the values obtained with the baseline catalyst model.
(2) In the optimal design for the higher inlet gas temperature, faster catalyst light-off occurs at a higher cell density and a smaller monolith radius because the light-off performance of the catalyst is increasing due to the convective heat transfer between gas and solid phases rather than by the heat capacity of the solid phase. Here, the light-off time and cumulative CO emissions are reduced by approximately 62% and 63%, respectively.
(3) In the optimal design for the higher inlet gas mass flow rate of 0.06 kg/s, the light-off time and CO cumulative emissions for optimal monolith geometry are reduced by approximately 72% and 75%, respectively. It can be seen that the light-off performance of the catalyst deteriorates compared to that of the gas flow rate of 0.04 kg/s, primarily due to the attendant decrease in the contact time between the catalyst and exhaust gas.
(4) In the optimal design for the axial catalyst distribution, the catalyst surface area of the optimal distributions is higher in the upstream section, while in the downstream section it is lower than that of the uniform distribution. Here, the light-off time and cumulative CO emissions are reduced by approximately 63% and 60%, respectively, as compared to those obtained with the uniform catalyst distribution.

REFERENCES

Baratti, R., Feckova, V., Morbidelli, M. and Varma, A. (1997). Optimal catalyst activity profiles in pellets. 11. the case of multiple-step distributions. *Ind. Eng. Chem. Res.* **36**, **8**, 3416–3420.

Bella, G., Rocco, V. and Maggiore, M. (1991). A study of inlet flow distortion effects on automotive catalytic converters. *ASME J. Eng. Gas Turb. Pow.*, **113**, 419–426.

Bird, R. B., Stewart, W. E. and Lightfoot, E. N. (1960). *Transport Phenomena.* 2nd edn. John Wiley & Sons. New York.

Brisley, R. J., Chandler, G. R., Jones, H. R., Anderson, P. J. and Shady, P. J. (1995). The use of palladium in advanced catalysts. *SAE Paper No.* 950259.

Chakravarty, S., Mittra, R. and Williams, N. R. (2002). Application of a microgenetic algorithm (MGA) to the design of broad-band microwave absorbers using multiple frequency selective surface screens buried in dielectrics. *IEEE Trans. Ant. Propa.* **50**, **3**, 284–296.

Church, M. L., Thoss, J. E. and Fizz, L. D. (1991). Operating temperature effects on catalyst performance and durability. *SAE Paper No.* 910845.

Koltsakis, G. C. and Stamatelos, A. M. (1997). Catalytic automotive exhaust aftertreatment. *Prog. Energy Combust. Sci.* **23**, **1**, 1–39.

Harada, K., Shimizu, R., Kurita, K. and Muramatsu, M. (1992). Development of air-assisted injector system. *SAE Paper No.* 920294.

Hauber, T., Zache, P., Braun, J. and Ueberschar, D. (1998). Influence of the space between monoliths and the geometry of endcones on the conversion rate of a catalytic converter. *SAE Paper No.* 980424.

Heibel, A. and Spaid, M. A. A. (1999). A new converter concept providing improved flow distribution and space utilization. *SAE Paper No.* 1999-01-0768.

Heimrich, M. J., Smith, L. R. and Kitowski, J. (1992). Cold-start hydrocarbon collection for advanced exhaust emission control. *SAE Paper No.* 920847.

Jeong, S. J. and Kim, W. S. (2000). Three-dimensional numerical study on the use of warm-up catalyst to improve light-off performance. *SAE Paper No.* 2000-01-0207.

Jeong, S. J. and Kim, W. S. (2001). A new strategy for improving the warm-up performance of a light-off auto-catalyst for reducing cold-start emissions. *Proc. Inst. Mech. Eng., D, J. Automob. Eng.* **215**, **11**, 1179–1196.

Jeong, S. J. and Kim, W. S. (2002). Simulation of thermal and flow characteristics for optimum design of an automotive catalytic converter. *Chem. Eng. Commun.* **189**, **10**, 1314–1339.

Jeong, S. J. and Kim, W. S. (2003). A study on the optimal monolith combination for improving flow uniformity and warm-up performance of an auto-catalyst. *Chem. Eng. Process.* **42**, **11**, 879–895.

Kim, J. Y. and Son, S. H. (1999). Improved flow efficiency of a catalytic converter using the concept of radially variable cell density - Part I. *SAE Paper No.* 1999-01-0769.

Ma, T., Collings, N. and Hands, T. (1992). Exhaust gas ignition (EGI) - a new concept for rapid light-off of automotive exhaust catalyst. *SAE Paper No.* 920400.

Martin, A. P., Will, N. S., Bordet, A., Cornet, P., Gondoin, C. and Mouton, X. (1998). Effect of flow distribution on emission performance of catalytic converters. *SAE Paper No.* 980936.

Melis, S., Varma, A. and Pereira, C. J. (1997). Optimal distribution of catalyst for a case involving heterogeneous and homogeneous reactions. *Chem. Eng. Sci.* **52**, **2**, 165–169.

Oh, S. H. and Cavendish, J. C. (1982). Transients of monolithic catalytic converters: response to step changes in feedstream temperature as related to controlling automobile emissions. *Ind. Eng. Chem. Prod. Res. Dev.* **21**, **1**, 29–37.

Psyllos, A. and Philippopoulos, C. (1993). Performance of a monolithic catalytic converter used in automotive emission control: the effect of longitudinal parabolic active metal distribution. *Ind. Eng. Chem. Res.* **32**, **8**, 1555–1559.

Summers, J. C., Hiera, J. P. and Williamson, W. B. (1991). Noble metal usage reduction strategies for three-way emission control catalysts. *SAE Paper No.* 911732.

Summers, J. C., Skowron, J. F. and Miller, M. J. (1993). Use of light-off catalysts to meet the California LEV/ULEV standards. *SAE Paper No.* 930386.

Tronci, S., Baratti, R. and Gavriiilidis, A. (1999). Catalytic converter design for minimisation of cold-start emissions. *Chem. Eng. Commun.*, **173**, 53–77.

Voltz, S. E., Morgan, C. R., Liederman, D. and Jacob, S. M. (1973). Kinetic study of carbon monoxide and propylene oxidation on platinum catalysts. *Ind. Eng. Chem. Prod. Res. Dev.* **12**, **4**, 294–301.

Whittenberger, W. A. and Kubsh, J. E. (1990). Recent developments in electrically heated metal monoliths. *SAE Paper No.* 900503.

Zarowski, C. J. (2004). *An Introduction to Numerical Analysis for Electrical and Computer Engineers.* John Wiley & Sons. New York.